molecular pharmaceutics

Article

Synthesis and Evaluation of 131I-skyrin as a Necrosis Avid Agent for Potential Targeted Radionuclide Therapy of Solid Tumors

Cong Wang, Qiaomei Jin, Shengwei Yang, Dongjian Zhang, Qin Wang, Jindian Li, Shaoli Song, Ziping Sun, Yicheng Ni, Jian Zhang, and Zhiqi Yin

Mol. Pharmaceutics, **Just Accepted Manuscript** • DOI: 10.1021/acs.molpharmaceut.5b00630 • Publication Date (Web): 08 Dec 2015

ACS Publications

Molecular Pharmaceutics is published by the American Chemical Society. 1155 Sixteenth Street N.W., Washington, DC 20036

Synthesis and Evaluation of ^{131}I-skyrin as a Necrosis Avid Agent for Potential Targeted Radionuclide Therapy of Solid Tumors

Cong Wang,[†,‡] Qiaomei Jin,[‡] Shengwei Yang[‡], Dongjian Zhang,[‡] Qin Wang,[‡,§] Jindian Li,[†,‡] Shaoli Song,[∥] Ziping Sun,[⊥] Yicheng Ni,[#] Jian Zhang,*[,‡] Zhiqi Yin,*[†]

[†]Department of Natural Medicinal Chemistry & State Key Laboratory of Natural Medicines, China Pharmaceutical University, Nanjing 210009, Jiangsu Province, P.R.China

[‡]Laboratories of Translational Medicine, Jiangsu Province Academy of Traditional Chinese Medicine, Nanjing 210028, Jiangsu Province, P.R.China

[§]College of Pharmacy, Nanjing University of Chinese Medicine, Nanjing, Jiangsu, China

[∥]Department of Nuclear Medicine, the Affiliated Renji Hospital of Shanghai Jiaotong University

[⊥]Radiation Medical Institute, Shandong Academy of Medical Sciences, Jinan 250062, Shandong Province, P.R.China

[#]Theragnostic Laboratory, Campus Gasthuisberg, KU Leuven, 3000 Leuven, Belgium

ABSTRACT

An innovative anticancer approach targeted to necrotic tissues, which serves as a noncancerous and generic anchor, may present a breakthrough. Necrosis avid agents with a flat conjugate aromatic structure selectively accumulate in necrotic tissues, but they easily forms aggregates that undesirably distribute to normal tissues. In this study, skyrin, a dianthraquinone compound with smaller and distorted π-cores and thus decreased aggregates as compared with Hypericin (Hyp), was designed to target necrosis for tumor therapy. Aggregation studies of skyrin by UV/Vis spectroscopy showed a smaller self-association constant with skyrin than with Hyp. Skyrin was labeled by Iodine-131 with a radiochemical purity of 95% and exhibited good stability in rat serum for 72 h. *In vitro* cell uptake studies showed significant difference in the uptake of ^{131}I-skyrin by necrotic cells than by normal cells ($P < 0.05$). Compared in rats with liver and muscle necrosis, radiobiodistribution, whole-body autoradiography and SPECT/CT studies revealed higher accumulation of ^{131}I-skyrin in necrotic liver and muscle ($p < 0.05$), but lower uptake in normal organs, relative to that of ^{131}I-Hyp. In mice bearing H22 tumor xenografts treated with combretastatin A4 disodium phosphate, the highest uptake of ^{131}I-skyrin was found in necrotic tumor. In conclusion, ^{131}I-skyrin appears a promising agent with reduced accumulation in nontarget organs for targeted radionuclide therapy of solid tumors.

KEYWORDS
necrosis, targeted radionuclide therapy, skyrin, ^{131}I, SPECT/CT, cancer

INTRODUCTION

Targeted therapies revitalized the field of cancer therapeutics with the promise of improved cure rates accompanied by reduced toxicity.[1] However, the unpredictable mutations, histological diversity and developed drug resistance of the growing tumor still impose challenges to target therapies.[2-4] Rather than directly targeting viable cancer cells, an innovative anticancer approach targeting to necrotic tissues may present a breakthrough.[5-7] Necrotic tissues, which locate always close to the viable cancer cells, comprise 30−80% of a fast-growing solid tumor[8-10] and the proportion can be even larger after certain anticancer therapies,[6, 11] can function as a generic anchor for targeting solid malignancies. In addition, necrotic tissues are noncancerous and more stable stromal targets that may confront less drug resistance.[7]

Necrosis avid agents (NAAs), a class of compounds that selectively accumulate in the necrotic tissues, have been explored over the past decade for estimating prognosis, assessing therapeutic responses to drug treatment and formulating therapeutic strategies.[12-15] To date, the majority of NAAs are developed for molecular imaging of necrotic tissues, such as hoechst-IR, zinc-dipicolylamine, ^{99m}Tc-glucarate etc. [16-18] only a handful are therapeutic or theragnostic agents.[7, 19]

Currently, Hypericin (Hyp, Figure 1B), a naphthodianthrone compound, is the most studied NAA and found to selectively accumulate in necrotic tissues with high necrotic-to-viable tissue ratios (up to 80).[20, 21] ^{131}I-Hyp has been proved as a promising theragnostic radiopharmaceutical with a high sustaining accumulation in tumor necrotic areas for cancer therapy.[7, 15, 19] However, Hyp easily forms aggregates in

aqueous environment,[22] which may strongly weaken the targeting biodistribution and lead to the undesired uptake in normal organs.[23, 24]

The aggregation of Hyp in aqueous solvent is mainly attributed to the strongly π-π interactions and hydrophobic effect of the nearly planar π-conjugate aromatic core (Figure 1D).[25, 26] Distorting π-conjugated system or reducing the size of π-cores will decrease the π-π stacking energy, making the formation of aggregates more difficult.[27, 28] Our groups recently synthesized protohypericin that has the same anthraquinone base structure but a smaller and slightly twisted aromatic core.[29] It presents a minor aggregation behavior and comparable necrosis affinity compared with Hyp.[29] However, protohypericin still tends to form aggregates and easily converts into Hyp under light.[29]

In order to further inhibit the aggregate formation, we designed skyrin (Figure 1A) that is a diphenyl compound sharing the same anthraquinone fragment but different molecular skeleton compared with Hyp. Due to the twisted π-cores, the dihedral angle of skyrin is 81.25°[30](22.96° for Hyp). Hence, we speculate that skyrin may share similar necrosis targetability, but present a dramatically reduced tendency in forming aggregates with better tissue distribution.

To validate this hypothesis, we synthesized and studied the hydrophilicity and aggregation of skyrin, preliminarily evaluated the necrosis avidity of ^{131}I-skyrin in rats with reperfused liver infarction (RLI) and ethanol-induced muscular necrosis (MN), and compared with Hyp (or ^{131}I-Hyp). Furthermore, the therapeutic potential of ^{131}I-skyrin was assessed on a H22 murine hepatoma mouse model.

EXPERIMENTAL SECTION

General. All reagents and solvents used were purchased from Sinopharm Chemical Reagent Co., Ltd (Shanghai, China) or Nanjing Chemical Reagent Co., Ltd (Nanjing, China) with the exception of Emodin (purity > 98%), which was purchased from Chengdu Huaxia Chemical Reagent Co., Ltd (Chengdu, China), and Hyp (purity > 98%), which was purchased from Chengdu Biopurify Phytochemicals Ltd (Chengdu, China). Iodogen (1, 3, 4, 6-tetrachloro-3α, 6α-diphenylglycouril) was obtained from Pierce Biotechnology (ZI Camp Jouven, France). Sodium iodide ($Na^{131}I$) was supplied by HTA Co., Ltd (Beijing, China) with a radionuclidic purity over 99% and the specific activity was 370 MBq/mL. Gadolinium-based contrast agent Magnevist was obtained from Bayer Schering Pharma AG (Berlin, Germany). The human hepatoma cell line HepG2 and murine hepatoma cell line H22 were obtained from American Type Culture Collection (Manassas, VA). Kunming mice (25−28 g) and Sprague Dawley (SD) rats (250−300 g) were furnished by Experimental Animal Center, Jiangsu Academy of Traditional Chinese Medicine (Nanjing, China). Animal procedures utilizing rats and mice were approved by the Institutional Animal Care and Use Committee.

All reaction mixtures were monitored using thin layer chromatography (TLC) on silica gel 60 F_{254} plates (Merck, Germany), and visualized by ultraviolet (UV) irradiation at 254 nm or staining with aluminum chloride or magnesium acetate. The synthesized compounds were purified by silica gel chromatography and Sephadex LH20. Sep-Pak plus C_{18} cartridges (Waters, USA) were preconditioned with ethanol (2 mL)

and water (2 mL) before use. ^{1}H and ^{13}C NMR spectra were carried out on a Bruker 300 MHz NMR (Switzerland) at 303K using DMSO-d_6 as an internal standard. Chemical shifts were reported in parts per million (δ, ppm) values. Electrospray-ionization mass spectrometry (ESI-MS) was carried out on HP1100 mass spectrometer (Agilent, Santa Clara, CA, USA). Reversed-phase high performance liquid chromatography (RP-HPLC) was performed on a Waters Alliance 2695 Separations module equipped with Waters 2998 UV/Visible detector (Waters Cooperation, Milford, MA, USA) and Berthold HERM LB500 radiometric detector (Millipore, Billerica, MA, USA). The RP-HPLC column was GRACE Alltima^{TM} C18 analytical column (250 mm × 4.6 mm, 5 μm). The radiochemical purity was assayed by analytical HPLC using methanol and water containing 0.04% ammonium acetate (v/v = 70:30 for ^{131}I-skyrin and 88:12 for ^{131}I-Hyp) in an isocratic mode at a flow rate of 1 mL/min under the column temperature of 30 °C. Magnetic resonance imaging (MRI) was performed using a 1.5T whole-body MR magnet (Echo speed; GE Co., NY).

Synthetic Approach.

Synthesis of Skyrin. The synthesis of emodinbianthrone was performed using emodin as the starting material as reported in the literature[31] (Scheme 1). Then emodinbianthrone (100 mg) was dissolved in 0.2 M potassium hydroxide solution (100 mL). The solution was heated at 100 °C, while a strong stream of oxygen was passed through it for 10 min. Then the solution was poured into excess 2 M hydrochloric acid, the red precipitate was so obtained and subjected to silica gel column chromatography (chloroform: methanol = 55:1) to give compound **4**. Yield: 53 mg, 52%. The final

product was characterized by ^{1}H, ^{13}C NMR and mass spectrometry. ^{1}H NMR (300 MHz, DMSO-d_6) δ (ppm): 2.32 (s, 6H, CH_3), 6.72 (s, 2H, H-7,7'), 7.12 (s, 2H, H-4,4'), 7.27 (s, 2H, H-2,2'), 11.14 (brs, 2H, OH), 12.01, 12.77 (s, 4H, OH); ^{13}C NMR (75 MHz, DMSO-d_6) δ (ppm): 21.49 (CH_3), 107.23 (CH), 109.01 (C), 113.10 (C), 120.42 (CH), 123.45 (CH), 123.51 (C), 131.29 (C), 133.23 (C), 148.17 (C), 161.05 (C), 164.35 (C), 181.99 (CO), 189.63 (CO); HR-ESI-MS: calculated for $[C_{30}H_{18}O_{10}]$: 538.0900, found $[M-H]^-$: 537.0824.

Synthesis of ^{127}I-Skyrin. Iodine (25 mg) was added to a stirred suspension of skyrin (107 mg) in a mixed solvent of tetrahydrofuran (THF, 15 mL) and H_2O (15 mL) at 0°C. Then $NaHCO_3$ (25 mg) was stepwise added and the mixture was stirred for 30 min. CH_3COOCH_3 (300 mL) was used to extract the organic phase. Purification of the reaction mixture was carried out using silica gel column chromatography (chloroform: methanol = 100:1) and Sephadex LH20 column chromatography. Compound 5 was obtained as a red powder (13 mg, 10%). 1H NMR (300 MHz, DMSO) δ (ppm): 2.29 (s, 3H, CH_3), 2.33 (s, 3H, CH_3), 6.69 (s, 1H, H-7'), 7.04, 7.13 (s, 2H, H-4,4'), 7.19, 7.27 (s, 2H, H-2,2'), 12.07, 12.79 (s, 2H, OH); HR-ESI-MS: calculated for $[C_{30}H_{17}O_{10}I]$: 663.9866, found $[M-H]^-$: 662.9801.

Aggregation Studies by UV/Vis Spectroscopy. The UV/Vis spectras of skyrin and Hyp were carried out using a Cary 5000 spectrophotometer (Varian, Australia).[22] Measurements were conducted in the function of concentration ranging from 1.3×10^{-6} M to 2.7×10^{-5} M at 20 °C, in water solution containing 50% DMSO. The measurements were carried out at wavelength ranging from 300 to 800 nm. The apparent

molar absorption coefficients at suitable wavelengths were fitted by nonlinear least-square regression analysis to the isodesmic (equal K) model according to equation (1)

$$A(\lambda, C) = [\varepsilon_M(\lambda) - \varepsilon_A(\lambda)]\left(\frac{2K_aC+1-\sqrt{4K_aC+1}}{2{K_a}^2C}\right) + \varepsilon_A(\lambda)C \quad (1)$$

Where A(λ,C) - absorbance at wavelength λ of the measured sample at the concentration of C in solution; $\varepsilon_M(\lambda)$ and $\varepsilon_A(\lambda)$ - the extinction coefficients for the monomeric and the aggregated compounds, respectively; Ka - aggregation constants.

The degree (or fraction) of aggregated molecules α_{agg} can be obtained according to the following equation (2), where c_T is the concentration of the compound.

$$\alpha_{agg} = 1 - \frac{2KC_T+1-\sqrt{4KC_T+1}}{2K^2{C_T}^2} \quad (2)$$

^{131}I Radiolabeling. In order to prolong the time of evaluation and investigate the potential for therapy, we choose Iodine-131 that has a longer half-life than Iodine-123 (8 days vs 13 h) and emits γ-rays and β-particles for imaging diagnosis and tumor internal radiotherapy. The Iodogen coating method was employed to radioiodinate skyrin/Hyp to form ^{131}I-skyrin/^{131}I-Hyp. Briefly, the water-insoluble oxidant "Iodogen" was dissolved in dichloromethane and coated on the walls of the Eppendorf tube. Radioiodination was conducted by adding 14.8 MBq of Na^{131}I and 1×10^{-7} mol of skyrin/Hyp dissolved in 300 μl dimethylsulfoxide (DMSO). Afterwards, the mixture was incubated at 30 °C for 20 min, and the reaction was terminated by transference of reaction solution to another clean tube. The product was passed through a Sep-Pak C_{18} cartridge, washed with 1 mL of water and eluted with 1 mL of methanol. The methanol eluent was collected and assayed by analytical HPLC using the conditions as de-

scribed above with ^{127}I-skyrin as a reference.

Stability Studies in Rat Serum. For *in vitro* stability study, 0.1 mL of the solution of ^{131}I-skyrin or ^{131}I-Hyp (7.4 MBq) was added to 0.9 mL of rat serum and incubated at 37 °C for 72 h. Plasma proteins were precipitated by adding 300 μL of ethanol and removed by centrifugation (12000 rpm, 8 min). The radiochemical stability was assayed by HPLC using the isocratic analysis method.

Octanol-Water Partition Coefficient. Log P was determined at physiological condition by the "shake-flask" method.[32] ^{131}I-skyrin or ^{131}I-Hyp (10 μL, 1.85 MBq) was added to a solution containing octanol (500 μL) and phosphate-buffered saline (PBS, 500 μL, pH 7.4). The resulting solution was vigorously vortexed at room temperature for 3−5 min and then centrifuged at 14000 rpm for 5 min. The counts in 10 μL aliquots of both octanol and saline phases were measured on a γ counter (PerkinElmer 1480; Waltham, MA). Two independent experiments were performed in triplicate. The octanol/buffer partition coefficient P was calculated as P = (cpm in the organic phase − background cpm)/(cpm in the aqueous phase − background cpm). The partition coefficient value was expressed as log P.

***In Vitro* Cell Binding Assay.** The HepG2 cells were seeded into a 6-well cell culture plate at a density of 5×10^5 cells/well and incubated at 37 °C in a humidified CO_2 incubator (5% CO_2) in RPMI 1640 supplemented with 10% fetal bovine serum (FBS) and 1% (v/v) penicillin/streptomycin overnight. After being washed with PBS containing 10% FBS, cells were incubated for 1 h under intense hyperthermia at 57 °C to induce necrosis[33] and at 37 °C as a control. Then the cells were transferred into 4 mL

Eppendorf tubes and co-incubated at 37 °C for 15 min with 37 KBq of ^{131}I-skyrin or ^{131}I-Hyp in 1 mL of RPMI-1640 medium. After incubation, the mixture was transferred into 1.5 mL tubes and centrifuged at 12000 rpm for 10 min. Then the tubes were frozen in liquid nitrogen, the bottom tips containing the cell pellet were cut off, and the cell pellets and supernatants were collected and the radioactivity was measured using a gamma counter. The radioactivity values were calculated and expressed as the percentage uptake per 10^8 cells. Experiments were performed twice with triplicate wells.

Animal Models of Necrosis

Rat Model of Reperfused Liver Infarction and Muscular Necrosis (RLI&MN). RLI&MN was conducted as previously described.[34] Simply, male SD rats were anaesthetized with intra-peritoneal injection of sodium pentobarbital at a dose of 40 mg/kg. Under laparotomy, the hilum of the right liver lobes was ligated with a suture to generate ischemia for 3 h. Then released hepatic inflow obstruction and massaged the liver lobe for reperfusion, and closed the abdominal cavity with two-layered sutures. The coexisting normal liver lobes were used as control for intra-individual comparison.

As a sclerotic agent, ethanol is used for tumor ablation in human patients and inducing tissue necrosis for optical imaging studies.[17] Each RLI model rat was intramuscularly injected with 0.2 mL ethanol in the left leg for creating chemically induced muscle necrosis, and animals were allowed to recover for 6−8 h after the procedure.

***In Vivo* Tumor Models.** Induction of necrosis in an H22 hepatocarcinoma cancer model was achieved as described previously with minor modification.[7] Briefly, mice were injected subcutaneously in the unilateral flank region with 1×10^7 H22 cells. Tumor volume was determined by caliper measurements with the formula: tumor volume = (minimum diameter)^2 × (maximum diameter) × 1/2. When the tumors reached approximately 6 to 8 mm in diameter (2−3 weeks), mice were injected via the tail vein with Combretastatin A4 disodium phosphate (CA4P) at a dose of 10 mg/kg. MRI was performed to evaluate whether the necrosis model was successful or not. See the supplemental material for the detailed procedures.

Tracer Administration. The thyroid of model rats and mice was blocked with Lugol's solution (1.2 g/L) in their drinking water 3 days before and till the end of experiment. In order to facilitate the administration, the reaction solution was diluted with polyethylene glycol 400 (PEG400) and propylene glycol (v/v =1:1) to formulate preparations immediately before injection. Each rats and mice was administrated intravenously with ^{131}I-skyrin or ^{131}I-Hyp formulation (14.8 MBq/Kg) for *in vivo* animal experiments.

Biodistribution Studies. For biodistribution studies, 24 model rats of RLI&MN (n = 4/group) were intravenously administered with ^{131}I-skyrin or ^{131}I-Hyp under anaesthesia and sacrificed at 12 h, 24 h and 72 h p.i., respectively. Organs of interest were removed, weighed, and counted for radioactivity using a γ counter. The decay-corrected activity per mass of tissue was calculated. Uptake of the tracers was calculated as the percentage of the injected dose per gram of tissue (% ID/g) with the

values expressed as mean ± standard deviation (SD) and percentage of injected dose (% ID) with the values expressed as mean ± SD.

***Ex vivo* Autoradiography and Histochemical Staining.** For *ex vivo* autoradiography studies, representative tissues of necrotic liver, normal liver and necrotic muscle at each time point were removed and washed thoroughly with 0.9% saline (4 °C) to remove blood pool activity. Sections of 10 and 30 μm were cut using a cryostat microtome (Shandon Cryotome FSE, Thermo Fisher Scientific Co., MA) at −20 °C and were thaw-mounted on glass slides. Autoradiographs of these slides were obtained by exposing the sections for 6−32 h to a high performance phosphor screen (Cyclone; Canberra-Packard, Ontario, Canada). After the exposure, the screen was read using a Phosphor Imager scanner and analyzed using Optiquant software (Cyclone^{TM}, Canberra-Packard, CT). Relative tracer concentration was estimated by regions of interest (ROI) analysis for the necrotic and viable tissues on all autoradiographs. The slides were stained with haematoxylin-eosin (H&E) using a conventional procedure and digitally photographed to confirm the presence or absence of necrosis. Photomicrographs were obtained from an optical microscope (Axioskop; Zeiss, Oberkochen, Germany) with magnification at × 200.

SPECT/CT Imaging Studies. The tomographic acquisitions were done on a combined SPECT/CT scanner (Precedence 6; Philips, The Netherlands) which hybrids a stand-alone dual-head γ-camera equiped with a pinhole high-energy collimator with a 6-slice spiral CT camera installed within the same gantry. Model rats (n = 3/group) were injected via the tail vein with approximately 3.7 MBq (100 μCi) of ^{131}I-skyrin or

^{131}I-Hyp. At 12 h, 24 h and 72 h p.i., rats were anesthetized with sodium pentobarbital at a dose of 40 mg/kg and placed in the prone position near the center of the field of view (FOV) of the scanner. The following protocol was used for SPECT acquisition: 128 × 128 matrix, 180° SPECT with 6° steps, 25 s/frame and a variable radius of rotation adapting to the closest possible distance from the phantom surface. Prior to each CT imaging, 0.1 mL Iobitridol was injected intravenously. For CT image acquisition, the scan parameters were 240 mA, 120 kV, a rotation time of 0.75 s, and 1mm slice thickness and a 0.5 × 1.5 mm collimation. Both SPECT and CT data were reconstructed and displayed as transaxial and coronal slices using an Astonish bone application package (Philips, The Netherlands). The SPECT and CT fusion images were obtained using the Syntegra software (Philips, The Netherlands).

Whole-body Autoradiography. For whole-body autoradiography studies, 6 model rats of RLI were intravenously injected with 3.7 MBq (100 μCi) of ^{131}I-skyrin or ^{131}I-Hyp. At 72 h p.i., rats were euthanized with overdose of sodium pentobarbital, embedded in 4% carboxymethylcellulose and stored at −20 °C until sectioning. Individual rat legs were removed, and coronal sections of 150 μm thickness were obtained using a cryostat macrotome (Leica SM2500, Wetzlar, Germany) at −20 °C. Sections were lyophilized and mounted on clear tape and exposed at −20 °C for 0.5−2 h to phosphor-imaging plates. Autoradiographic images were obtained and analyzed as described above.

Experiment on Mice Bearing H22 Tumors. The mice received ^{131}I-skyrin (15 μCi) 24 h after CA4P treatment. Twenty mice (n = 10/group) were sacrificed at 24 h and 72

h p.i. for biodistribution studies, whole-body autoradiography, ex vivo autoradiography and histochemical staining as described above.

Statistical analysis. Numerical results were reported as the mean ± SD. Means were compared using Student's t test and groups with a P value less than 0.05 were considered significant differences.

RESULTS

Chemistry. Skyrin and ^{127}I-skyrin were synthesized as shown in Scheme 1. Compound 2 was synthesized using tin (II) chloride hydrate in high yield. Coupling of emodin anthrone was realized using iron (III) chloride hydrate as the catalyst and skyrin was obtained when emodin bianthrone dissolved in alkali solution in the presence of sufficient quantities of oxygen. In all cases, intermediate and final products were purified on silica gel or Sephadex LH20 column chromatography and the > 95% purity was verified by RP-HPLC.

Aggregation in Water-DMSO. For a comparison of the aggregation behaviour of skyrin and Hyp, water-DMSO (1:1) proved to be an ideal solvent. Hyp is insoluble in water that is the main components of blood, DMSO appears an ideal solvent to introduce it into the aqueous medium and was chosen to dissolve Hyp. The aggregation constants of skyrin and Hyp determined according to the isodesmic model were (3.17 ± 0.52) × 10^5 M^{-1} and (1.13 ± 0.34) × 10^6 M^{-1}, respectively. Figure 2 presents the concentration-dependent transitions from monomeric to aggregated molecules and the calculated regression lines according to the isodesmic model. All these indicated a downward tendency in forming aggregates of skyrin compared that of Hyp.

Radiochemistry. ^{131}I labeling was performed in a straightforward method with a preparation time of 20 min for ^{131}I-skyrin/^{131}I-Hyp at room temperature. After purification, the specific activity of ^{131}I tracers were typically about 5-10 Ci/mmol. Radiochemical purity greater than 98% (labeling yield more than 90%) could be obtained as measured by analytic RP-HPLC for both tracers. The structure of ^{131}I-skyrin was de-

termined by using ^{127}I-skyrin as reference compound (Figure 3).

Partition Coefficient and *in Vitro* Stability. The partition coefficient, log P (pH 7.4), of ^{131}I-skyrin and ^{131}I-Hyp were measured as 1.88 ± 0.08 (n = 3) and 2.76 ± 0.03 (n = 3), respectively. For *in vitro* serum stability analysis, both tracers were intact for 72 h at 37 °C in rat serum (Figure 3), suggesting that they had very good stability *in vitro*.

***In Vitro* Binding to Necrotic Cells.** Cell binding of ^{131}I-skyrin and ^{131}I-Hyp were performed using HepG2 cells and the results are shown in Table 1. Both tracers were found to have a significantly higher uptake with hyperthermia treated cells compared to non-treated cells ($P < 0.05$). The ratios of radioactivity in the pellet for the treated cells compared to non-treated cells were 3.52 ± 0.70 for ^{131}I-skyrin and 3.79 ± 0.61 for ^{131}I-Hyp.

Biodistribution. The biological distribution results of ^{131}I-skyrin and ^{131}I-Hyp in rat models with RLI&MN were showed in Table 2 and Table S1. ^{131}I-skyrin had high uptake in necrotic tissues (3.19 ± 0.64% ID/g for necrotic liver and 1.52 ± 0.48% ID/g for necrotic muscle at 12 h p.i., respectively) and good retention (3.85 ± 0.27% ID/g for necrotic liver and 1.21 ± 0.36% ID/g for necrotic muscle at 72 h p.i., respectively). Necrotic to viable liver and muscle ratios increased from 6.06 ± 1.27 and 4.92 ± 1.18 at 12 h to 20.87 ± 3.98 and 10.59 ± 0.84 at 72 h. Except for the blood, the clearance of ^{131}I-skyrin from the nontarget tissues was fast and the accumulations were lower than 0.8% ID/g at 12 h p.i. in most of the examined normal organs.

When compared with ^{131}I-skyrin, ^{131}I-Hyp had comparable necrotic liver uptake at

earlier time points but lower at later time points. ^{131}I-Hyp also showed lower uptake in necrotic muscle but higher lung and spleen accumulation ($P < 0.05$). For all of the other tissues, these two radiotracers showed comparable radioactivity uptake except slower blood clearance with ^{131}I-skyrin ($P < 0.05$).

Autoradiography and Histochemical Staining. Representative autoradiographic images (upper row), photographs (lower row) and photomicrographs (bottom row) of the corresponding H&E stained slices of necrotic muscle, necrotic liver and normal liver slices comparing two tracers at 24 h p.i. are shown in Figure 4. On H&E stained slices, purple areas correspond to viable tissue while pink areas correspond to necrotic tissue. The radioactivity signal from both ^{131}I-skyrin and ^{131}I-Hyp colocalized with necrotic tissues detected with H&E assay. Analysis of the autoradiogram images (comparison of the DLU/mm^2 for necrotic and normal tissue) showed that both ^{131}I-skyrin and ^{131}I-Hyp were able to accurately delineate necrotic tissue with necrotic to viable tissue activity ratios up to 9−25/6−31 for the liver and 8−15/5−6 for muscle, respectively.

SPECT/CT Imaging. Representative coronal and transaxial SPECT/CT images of model rats of RLI&MN (n = 3/group) at 72 h after administration of ^{131}I-skyrin or ^{131}I-Hyp are shown in Figure 5. The enhanced CT displayed the necrotic liver/muscle with lower signal than normal due to the contrast agents (Iobitridol) inaccessible into necrotic areas. SPECT-CT showed that the necrotic liver and muscle could be clearly visualized after intravenous injection of ^{131}I-skyrin and demonstrated high contrast with low contralateral background. Most of the nontargeted organs demonstrated low

signal, indicating relatively low accumulation of the tracer. When compared with ^{131}I-skyrin, similar findings were observed with ^{131}I-Hyp except that there was no detectable uptake of ^{131}I-Hyp in necrotic muscle with high radioactivity accumulation in intestines.

Whole-body Autoradiography. Whole-body autoradiography proved as a preferred method for conducting tissue biodistribution studies. The autoradiographic results are compared in Figure 6. For both probes, the necrotic liver was the organ with the highest uptake, reflecting the extraordinary avidity in necrotic tissues. Relatively low uptake in the lung, gut cavities and high uptake in the heart (blood) was observed with ^{131}I-skyrin, which was in good agreement with the results of *ex vivo* biodistribution by γ counting.

Experiment on Mice Bearing H22 Tumors. Treatment of mice bearing tumors with CA4P induces substantial necrosis.[6] Spontaneous necrosis existed in H22 tumor, tumor necrosis ratio as measured from contrast enhanced T1-weighted (CE-T1W) images at baseline was about 17% (Figure S7 in the Supporting Information) in each group. The necrosis ratio increased to 52% 24h after the CA4P treatment. ^{131}I-skyrin showed highest uptake in the necrotic tumors at both time points and the actual value of necrotic tumor should be higher due to the fact that viable cells were intermixed with necrotic cells (Table S2 in the Supporting Information). Whole-body and intratumoral distribution of ^{131}I-skyrin at 72 h in mice bearing H22 tumors were shown in both autoradiographic and H&E images (Figure 7). The highest uptake in tumor was clearly visualized after chemotherapy (Figure 7A and 7B). There was also relatively

high accumulation in the liver, but the tumor to liver was 3.49 ± 0.52 as determined by autoradiography. For slices of tumors, there was little signal in the viable tumors and the necrotic to viable ratio was up to 11.52 ± 1.25 (Figure 7C−F), which further confirmed the excellent necrosis affinity.

DISCUSSION

In the present study, we synthesized a tracer and evaluated its targetability to necrotic tissues, especially tumor necrosis for potential tumor therapy. Skyrin presented a better hydrophilicity and downward tendency in forming aggregates compared with Hyp, leading to its lower uptake in the monocyte macrophage system (MPS). Simultaneously encouraging result is that ^{131}I-skyrin showed prominent necrotic targetability with high sustaining necrotic to viable activity ratios.

Skyrin appeared less aggregative in aqueous solution by UV/Vis analysis with a self-association constant that is less than one third of the corresponding value of Hyp. The aggregation of molecules might be affected by many factors such as solvent, the size and electronic nature of the π-conjugated system and the peripheral substituents attached to the π-conjugated core.[35-37] Dispersion forces, an important contributor to the overall energy of π-π interactions, are favored by increased surface areas. Accordingly, it is reasonable that skyrin with a decreased core size had a lower propensity to form aggregates. Furthermore, due to the twisted core, the π-π contact area may also dramatically reduce, which can be attributed to an increase of the π-π distance or a longitudinal displacement between aggregates. In addition, the hydrophobic effect of ^{131}I-skyrin, an important contribution to the Gibbs free aggregation energy, is also decreased with a smaller octanol-water partition coefficient. Hyp is poorly soluble and forms aggregates in aqueous environment. The coarse aggregates are intercepted by pulmonary capillary network and small ones are cleaned and retained in the liver and spleen. Liu *et al*. revealed that the non-aggregated formulation of Hyp showed higher

accumulation in target organ and lower accumulation in MPS compared with two aggregated formulations (over concentrated Hyp in DMSO and in water solution).[24] The lessened aggregation led to a significantly less radioactive uptake of ^{131}I-skyrin in the MPS than that of ^{131}I-Hyp, especially in the lung and spleen (0.40 ± 0.03% ID/g and 0.26 ± 0.07% ID/g vs 1.97 ± 0.20% ID/g and 1.05 ± 0.15% ID/g at 12 h p.i.). These were also clearly observed on the whole-body autoradiographic image, while ^{131}I-Hyp showed higher signal in the lung.

The necrosis targetability of ^{131}I-skyrin was preliminarily investigated and compared with ^{131}I-Hyp in model rats with RLI&MN to acquire reliable evidences. Acute and localized tissue damage in rats was achieved by injecting ethanol into the rear leg muscle and performing ischemia-reperfusion operation on the right liver lobe. Although this in vivo tissue necrosis model has limited relevance with clinic, it serves as a highly reproducible and reliable experimental system for quantitative comparison of radiolabeled probes.[17, 38] Both tracers showed high necrotic to viable tissue activity ratios (up to 20−24 for liver and 5−11 for muscle) and sustaining uptake in necrotic liver (3.85 ± 0.27% ID/g for ^{131}I-skyrin and 3.26 ± 0.23% ID/g for ^{131}I-Hyp, at 72 h). Although ^{131}I-skyrin had similar accumulation in necrotic liver at early time points, it had higher uptake at 72 h and in necrotic muscle than ^{131}I-Hyp. Encouraged by these results, ^{131}I-skyrin was then evaluated in xenograft model. Biodistribution studies, autoradiography and corresponding H&E demonstrated that ^{131}I-skyrin may accumulate highly in necrotic tumors and be a promising agent for cancer therapy.

The similar higher uptake with hyperthermia treated cells compared to non-treated

cells indicated that both tracers had favourable necrosis targetability. Being a pronounced hydrophobic compound, ^{131}I-Hyp tended more to nonspecifically bind to cellular lipophilic membrane structures.[39, 40] Once cell become necrotic, the binding of ^{131}I-Hyp to the intracellular membrane structures added up. For these reasons, the absolute values of accumulation in both treated and non-treated cells for ^{131}I-Hyp seem to be higher.

Currently, the majority of targeted probes are designed to bind to the receptors overexpressed on the membrane of viable tumor cells. However, probes that targeted to the necrosis tissues are rare but have following advantages. Necrosis is widely present in numerous disorders or pathologies, including cardiac disease and cancer. Furthermore, probes can be designed with extraordinarily high avidity and specificity due to the failure of necrotic cells to preserve the integrity of cell membrane and exchange of macromolecules (such as exposed DNA, heat shock proteins, phosphatidylserine etc.) between the intracellular and extracellular environment which are absent in viable cells.[41] In addition, being more stable and generic targets with less heterogeneity and drug resistance, better disease diagnosis and therapeutic response can be acquired by attaching γ ray-emitting or β^- particle-emitting radioisotopes to the NAAs.

As a promising anticancer strategy has been applied in clinical treatment, tumor necrosis therapy (TNT) uses a genetically engineered, ^{131}I chimeric mAb, which targets naturally occurring nuclear antigen histone present only on dying or dead cells.[6] However, potential immunogenicity and poor stability owing to its property as a large protein have limited its clinical application.[42] Being a small molecule compound,

^{131}I-skyrin would show little immunogenicity as well as good stability.

Rational tumor combination therapy can improve treatment efficacy and enable the reduction of side effects.[43] Due to the insufficient blood supply, tumor necrosis is ubiquitous in the solid tumor as a result of hypoxia and lack of prompt clearance. However, the degree and location of necrosis is closely related to the type of the tumor and it is recommended to combine with other types of treatments. If radiofrequency ablation or chemotherapy drugs are first used to cause massive tumor necrosis, then NAAs carrying radioisotopes can be systemically delivered and specifically accumulate at intratumoral necrosis, irradiate the adjacent remnant tumor cells with β^- particle to prevent malignant cell repopulation. Being a promising molecular agent for clinical translation and future development, we plan to combine ^{131}I-skyrin with chemotherapy drugs for treating various solid tumors in future experiments. In addition, the exact mechanism of NAAs binding to necrotic tissues should be further elucidated and more efficient way of synthesis needs to be exploited.

CONCLUSIONS

In this study, ^{131}I-skyrin exhibited comparable necrosis targeting properties with ^{131}I-Hyp *in vitro* and *in vivo*. However, skyrin presented a smaller self-association constant compared with Hyp and the uptake of ^{131}I-skyrin in normal organs, especially lungs and spleen, was significantly reduced. In tumor models, ^{131}I-skyrin showed the highest uptake in chemotherapy-induced necrotic tumors. All these results indicate that ^{131}I-skyrin is a promising agent for targeted radionuclide therapy of solid tumors.

ASSOCIATED CONTENT

Supporting Information

^{1}H, ^{13}C NMR, high resolution mass spectra of skyrin and ^{127}I-skyrin. Biodistribution of ^{131}I-skyrin in rats of RLI&MN and CA4P treated liver cancer model. Magnetic resonance images of mice bearing H22 tumors before and 24 h after CA4P treatment. This material is available free of charge via the Internet at http://pubs.acs.org.

AUTHOR INFORMATION

Corresponding Author

*(J.Z.) Phone: +86-25-52362107. Fax: +86-25-85637817. E-mail: zjwonderful@hotmail.com.

*(Z.Y.) Phone: +86-25-86185371. Fax: +86-25-85301528. E-mail: chyzq2005@126.com.

Notes

The authors declare no competing financial interest.

ACKNOWLEDGMENT

This work was supported, in part, by the National Natural Science Foundation of China (No.81473120), the Ninth Batch of “Six Talent Peaks” Project of Jiangsu Province (No.2012-YY-008), and A Project Funded by the Priority Academic Program Development of Jiangsu Higher Education Institutions. We thank Mr Yinyan Zhu, Department of Nuclear Medicine, the Affiliated Renji Hospital of Shanghai Jiaotong University, for his wonderful work in SPECT/CT scanning.

ABBREVIATIONS

NAAs, necrosis avid agents; Hyp, Hypericin; SPECT/CT, single photon emission computed tomography/computed tomography; RP-HPLC, reverse phase-high performance liquid chromatography; RLI, reperfused liver infarction; MN, muscular necrosis; KI, potassium iodide; H&E, haematoxylin-eosin; p.i., postinjection; CA4P, combretastatin A4 disodium phosphate.

REFERENCES

(1) Nicolaides, N. C.; Sass, P. M.; Grasso, L. Advances in targeted therapeutic agents. *Expert Opin. Drug Discov.* **2010**, *5* (11), 1123-1140.

(2) Santhosh, S.; Kumar, P.; Ramprasad, V.; Chaudhuri, A. Evolution of targeted therapies in cancer: opportunities and challenges in the clinic. *Future Oncol.* **2015**, *11* (2), 279-293.

(3) Keefe, D. M.; Bateman, E. H. Tumor control versus adverse events with targeted anticancer therapies. *Nat. Rev. Clin. Oncol.* **2012**, *9* (2), 98-109.

(4) Merlo, L. M.; Pepper, J. W.; Reid, B. J.; Maley, C. C. Cancer as an evolutionary and ecological process. *Nat. Rev. Cancer* **2006**, *6* (12), 924-935.

(5) Ji, Y.; Jiang, C.; Zhang, X.; Liu, W.; Gao, M.; Li, Y.; Wang, J.; Wang, Q.; Sun, Z.; Jiang, X. Necrosis targeted combinational theragnostic approach to treat cancer. *Oncotarget* **2014**, *5* (10), 2934-2946.

(6) Chen, F. M.; Taylor, C. R.; Epstein, A. L. Tumor necrosis treatment of ME-180 human cervical carcinoma model with ^{131}I-labeled TNT-1 monoclonal antibody. *Cancer Res.* **1989**, *49* (16), 4578-4585.

(7) Li, J.; Sun, Z.; Zhang, J.; Shao, H.; Miranda Cona, M.; Wang, H.; Marysael, T.; Chen, F.; Prinsen, K.; Zhou, L. A dual-targeting anticancer approach: soil and seed principle. *Radiology* **2011**, *260* (3), 799-807.

(8) Shapiro, W. R.; Carpenter, S. P.; Roberts, K.; Shan, J. S. ^{131}I-chTNT-1/B mAb: tumour necrosis therapy for malignant astrocytic glioma. *Expert Opin. Biol. Ther.* **2006**, *6* (5), 539-545.

(9) Cooper, E.; Bedford, A.; Kenny, T. Cell death in normal and malignant tissues. *Adv. Cancer Res.* **1975**, *21*, 59-120.

(10) Kim, S.; Park, J.; Youn, Y. S.; Oh, K. T.; Bae, J. H.; Lee, E. S. Hoechst 33258-conjugated hyaluronated fullerene for efficient photodynamic tumor therapy and necrotic tumor targeting. *J. Bioact. Compat. Pol.* **2015**, *30* (3), 275-288.

(11) Song, W.; Tang, Z.; Zhang, D.; Yu, H.; Chen, X. Coadministration of Vascular Disrupting Agents and Nanomedicines to Eradicate Tumors from Peripheral and Central Regions. *Small* **2015**, DOI: 10.1002/smll.201500324.

(12) Li, J.; Chen, F.; Cona, M. M.; Feng, Y.; Himmelreich, U.; Oyen, R.; Verbruggen, A.; Ni, Y. A review on various targeted anticancer therapies. *Targ. Oncol.* **2012**, *7* (1), 69-85.

(13) Park, D.; Xie, B. W.; Van Beek, E. R.; Blankevoort, V.; Que, I.; Lowik, C. W. G. M.; Hogg, P. J. Optical Imaging of Treatment-Related Tumor Cell Death Using a Heat Shock Protein-90 Alkylator. *Mol. Pharmaceutics* **2013**, *10* (10), 3882-3891.

(14) Ni Y, Bormans G, Chen F, Verbruggen A, and Marchal G. Necrosis avid contrast agents: functional similarity versus structural diversity. *Investigative Radiology* **2005**, *40*(8): 526-535.

(15) Li, J.; Cona, M. M.; Chen, F.; Feng, Y.; Zhou, L.; Yu, J.; Nuyts, J.; de Witte, P.; Zhang, J.; Himmelreich, U; Verbruggen, A.; Ni, Y. Exploring theranostic potentials of radioiodinated hypericin in rodent necrosis models. *Theranostics* **2012**, *2* (10), 1010-1019.

(16) Dasari, M.; Lee, S.; Sy, J.; Kim, D.; Lee, S.; Brown, M.; Davis, M.; Murthy, N.

Hoechst-IR: an imaging agent that detects necrotic tissue in vivo by binding extracellular DNA. *Org. Lett.* **2010**, *12* (15), 3300-3303.

(17) Smith, B. A.; Gammon, S. T.; Xiao, S.; Wang, W.; Chapman, S.; McDermott, R.; Suckow, M. A.; Johnson, J. R.; Piwnica-Worms, D.; Gokel, G. W. In Vivo Optical Imaging of Acute Cell Death Using a Near-Infrared Fluorescent Zinc-Dipicolylamine Probe. *Mol. Pharmaceutics* **2011**, *8* (2), 583-590.

(18) Mariani, G.; Villa, G.; Rossettin, P.; Spallarossa, P.; Bezante, G.; Brunelli, C.; Pak, K.Y.; Khaw, B.A.; Strauss, H. Detection of acute myocardial infarction by ^{99m}Tc-labeled D-glucaric acid imaging in patients with acute chest pain. *J. Nucl. Med.* **1999**, *40* (11), 1832-1839.

(19) Li, J.; Cona, M. M.; Chen, F.; Feng, Y.; Zhou, L.; Zhang, G.; Nuyts, J.; de Witte, P.; Zhang, J.; Yu, J.; Oyen, R.; Verbruggen, A.; Ni, Y. Sequential Systemic Administrations of Combretastatin A4 Phosphate and Radioiodinated Hypericin Exert Synergistic Targeted Theranostic Effects with Prolonged Survival on SCID Mice Carrying Bifocal Tumor Xenografts. *Theranostics* **2013**, *3* (2), 127-137.

(20) Van de Putte, M.; Wang, H.; Chen, F.; de Witte, P. A.; Ni, Y. Hypericin as a marker for determination of tissue viability after intratumoral ethanol injection in a murine liver tumor model. *Acad. Radiol.* **2008**, *15* (1), 107-113.

(21) Fonge, H.; Vunckx, K.; Wang, H.; Feng, Y.; Mortelmans, L.; Nuyts, J.; Bormans, G.; Verbruggen, A.; Ni, Y. Non-invasive detection and quantification of acute myocardial infarction in rabbits using mono-[^{123}I] iodohypericin μSPECT. *Eur. Heart J.* **2007**, *29* (2), 260-269.

(22) Pietrzak, M.; Maciejczyk, M.; Szabelski, M.; Kasparek, A.; Wieczorek, Z. Self-association of hypericin analyzed by light absorption and fluorescence spectroscopy and molecular dynamics simulations. *Chem. Phys. Lett.* **2014**, *601*, 39-44.

(23) Van De Putte, M.; Roskams, T.; Bormans, G.; Verbruggen, A.; De Witte, P. A. The impact of aggregation on the biodistribution of hypericin. *Int. J. Oncol.* **2006**, *28* (3), 655-660.

(24) Liu, X.; Jiang, C.; Li, Y.; Liu, W.; Yao, N.; Gao, M.; Ji, Y.; Huang, D.; Yin, Z.; Sun, Z; Ni, Y.; Zhang, J. Evaluation of Hypericin: Effect of Aggregation on Targeting Biodistribution. *J. Pharm. Sci.* **2015,** *104* (1), 215-222.

(25) Falk, H.; Meyer, J. On the homo- and heteroassociation of hypericin. *Monatshefte für Chemie / Chemical Monthly* **1994**, *125* (6), 753-762.

(26) Bánó, G.; Staničová, J.; Jancura, D.; Marek, J.; Bánó, M. s.; Uličný, J.; Strejčková, A.; Miškovský, P. On the Diffusion of Hypericin in Dimethylsulfoxide/Water Mixtures - The Effect of Aggregation. *J. Phys.Chem. B* **2011**, *115* (10), 2417-2423.

(27) Foster, E. J.; Jones, R. B.; Lavigueur, C.; Williams, V. E. Structural factors controlling the self-assembly of columnar liquid crystals. *J. Am. Chem. Soc.* **2006**, *128* (26), 8569-8574.

(28) Chen, Z.; Baumeister, U.; Tschierske, C.; Würthner, F. Effect of Core Twisting on Self-Assembly and Optical Properties of Perylene Bisimide Dyes in Solution and Columnar Liquid Crystalline Phases. *Chemistry-a European Journal* **2007**, *13* (2),

450-465.

(29) Liu, X.; Feng, Y.; Jiang, C.; Lou, B.; Li, Y.; Liu, W.; Yao, N.; Gao, M.; Ji, Y.; Wang, Q. Radiopharmaceutical evaluation of ^{131}I-protohypericin as a necrosis avid compound. *J. Drug Target.* **2015**, *23* (5), 417-426.

(30) *Gaussian 98*, Gaussian Inc., Pittsburgh, PA, USA.

(31) Motoyoshiya, J.; Masue, Y.; Nishi, Y.; Aoyama, H. Synthesis of hypericin via emodin anthrone derived from a two-fold diels-alder reaction of 1,4-benzoquinone. *Nat. Prod. Commun.* **2007**, *2* (1), 67-70.

(32) Zhao, Z.; Yu, Q.; Mou, T.; Liu, C.; Yang, W.; Fang, W.; Peng, C.; Lu, J.; Liu, Y.; Zhang, X. Highly efficient one-pot labeling of new phosphonium cations with fluorine-18 as potential PET agents for myocardial perfusion imaging. *Mol. Pharmaceutics* **2014**, *11* (11), 3823-3831.

(33) Perek, N.; Sabido, O.; Le Jeune, N.; Prevot, N.; Vergnon, J. M.; Clotagatide, A.; Dubois, F. Could ^{99m}Tc-glucarate be used to evaluate tumour necrosis? *Eur. J. Nucl. Med. Mol. Imag.* **2008**, *35* (7), 1290-1298.

(34) Zhang, D.; Huang, D.; Ji, Y.; Jiang, C.; Li, Y.; Gao, M.; Yao, N.; Liu, X.; Shao, H.; Jing, S., Experimental evaluation of radioiodinated sennoside B as a necrosis-avid tracer agent. *J. Drug Target.* **2014**, *23*, 180-190.

(35) Chen, Z.; Lohr, A.; Saha Möller, C. R.; Würthner, F. Self-assembled π-stacks of functional dyes in solution: structural and thermodynamic features. *Chem. Soc. Rev.* **2009**, *38*, 564-584.

(36) Fink, R. F.; Seibt, J.; Engel, V.; Renz, M.; Kaupp, M.; Lochbrunner, S.; Zhao,

H.-M.; Pfister, J.; Würthner, F.; Engels, B. Exciton trapping in π-conjugated materials: A quantum-chemistry-based protocol applied to perylene bisimide dye aggregates. *J. Am. Chem. Soc.* **2008**, *130* (39), 12858-12859.

(37) Chen, Z.; Fimmel, B.; Würthner, F. Solvent and substituent effects on aggregation constants of perylene bisimide π-stacks – a linear free energy relationship analysis. *Org. Biomol. Chem.* **2012**, *10* (30), 5845-5855.

(38) Wu, X.; Wang, H.; Chen, F.; Jin, L.; Li, J.; Feng, Y.; DeKeyzer, F.; Yu, J.; Marchal, G.; Ni, Y. Rat model of reperfused partial liver infarction: characterization with multiparametric magnetic resonance imaging, microangiography, and histomorphology. *Acta. Radiol.* **2009**, *50* (3), 276-287.

(39) Thomas, C.; Pardini, R. S., Oxygen dependence of hypericin-induced phototoxicity to EMT6 mouse mammary carcinoma cells. *Photochem Photobiol* **1984,** *39* (6), 831-837.

(40) Agostinis, P.; Vantieghem, A.; Merlevede, W.; de Witte, P. A., Hypericin in cancer treatment: more light on the way. *Int. J. Biochem. Cell B.* **2002,** *34* (3), 221-241.

(41) Smith, B. A.; Smith, B. D. Biomarkers and molecular probes for cell death imaging and targeted therapeutics. *Bioconjugate Chem.* **2012**, *23* (10), 1989-2006.

(42) Begg, A. C.; Stewart, F. A.; Vens, C. Strategies to improve radiotherapy with targeted drugs. *Nat. Rev. Cancer* **2011**, *11* (4), 239-253.

(43). Weiss, A.; Bonvin, D.; Berndsen, R. H.; Scherrer, E.; Wong, T. J.; Dyson, P. J.; Griffioen, A. W.; Nowak-Sliwinska, P. Angiostatic treatment prior to chemo- or

photodynamic therapy improves anti-tumor efficacy. *Sci. Rep.* **2015**, doi: 10.1038/srep08990.

Table 1. Accumulation of ^{131}I-skyrin and ^{131}I-Hyp in HepG2 cells

Compound	Cells	Mean ± SD % uptake/10^8 cells[b]
^{131}I-skyrin	Control	1.68 ± 0.56
	Treated[a]	5.66 ± 0.80
^{131}I-Hyp	Control	4.33 ± 0.75
	Treated[a]	16.14 ± 1.54

[a]Necrosis was induced in HepG2 cells by treatment under hyperthermia at 57°C.

[b]Each value is the mean ± SD % out of the three experiments.

Table 2. Biodistribution and the Necrotic-to-Normal Tissue Ratios of ^{131}I-skyrin and ^{131}I-Hyp in Liver and Muscular Necrosis Models (n= 4/Group)[a]

organ	12 h		24 h		72 h	
	^{131}I-skyrin	^{131}I-Hyp	^{131}I- skyrin	^{131}I-Hyp	^{131}I- skyrin	^{131}I-Hyp
blood	1.09 ± 0.15*	0.40 ± 0.07	0.89 ± 0.10*	0.23 ± 0.05	0.46 ± 0.06*	0.09 ± 0.02
brain	0.04 ± 0.01	0.03 ± 0.01	0.03 ± 0.01	0.01 ± 0.00	0.03 ± 0.00	0.01 ± 0.00
thyroid	0.25 ± 0.08	0.21 ± 0.05	0.24 ± 0.04	0.26 ± 0.04	0.17 ± 0.04	0.15 ± 0.04
lungs	0.40 ± 0.03*	1.97 ± 0.20	0.28 ± 0.04*	1.58 ± 0.13	0.22 ± 0.04*	1.06 ± 0.17
heart	0.19 ± 0.02*	0.62 ± 0.08	0.14 ± 0.03*	0.37 ± 0.05	0.10 ± 0.02*	0.20 ± 0.03
spleen	0.26 ± 0.07*	1.05 ± 0.15	0.16 ± 0.02*	0.69 ± 0.06	0.09 ± 0.02*	0.19 ± 0.03
stomach	0.29 ± 0.07	0.28 ± 0.05	0.16 ± 0.03	0.21 ± 0.05	0.11 ± 0.02	0.10 ± 0.03
pancreas	0.24 ± 0.07	0.36 ± 0.11	0.15 ± 0.04*	0.56 ± 0.16	0.13 ± 0.05*	0.49 ± 0.12
intestine	0.34 ± 0.06*	0.74 ± 0.12	0.25 ± 0.04*	0.63 ± 0.08	0.12 ± 0.04	0.23 ± 0.06
kidney	0.49 ± 0.06	0.35 ± 0.04	0.29 ± 0.04	0.23 ± 0.05	0.18 ± 0.05	0.16 ± 0.03
bone	0.15 ± 0.06*	0.25 ± 0.05	0.16 ± 0.03	0.16 ± 0.03	0.10 ± 0.03	0.08 ± 0.02
normal liver	0.73 ± 0.15	0.65 ± 0.09	0.37 ± 0.05	0.31 ± 0.05	0.19 ± 0.05	0.14 ± 0.02
necrotic liver	3.19 ± 0.64	3.35 ± 0.63	4.43 ± 0.68	4.06 ± 0.63	3.85 ± 0.27*	3.26 ± 0.23
normal muscle	0.31 ± 0.05	0.11 ± 0.04	0.18 ± 0.04	0.08 ± 0.01	0.11 ± 0.03	0.10 ± 0.03
necrotic muscle	1.52 ± 0.48*	0.44 ± 0.11	1.33 ± 0.46*	0.39 ± 0.10	1.21 ± 0.36*	0.34 ± 0.05
ratios						
NL/L[b]	6.06 ± 1.27	6.97 ± 1.61	11.89 ± 1.49	13.12 ± 2.50	20.87 ± 3.98	23.92 ± 2.32
NM/M[c]	4.92 ± 1.18	4.49 ± 1.59	7.49 ± 1.55	5.00 ± 0.13	10.59 ± 0.84	3.37 ± 0.66

[a]*$P < 0.05$, compared with ^{131}I-Hyp data at 12 h, 24 h and 72 h, respectively. Data are presented as % ID/g tissue ± SD (n = 4) after intravenous injection of the tracer (2.96−3.7 MBq) at 12 h, 24 h and 72 h (n = 4). [b]NL/L, necrotic liver/liver. [c]NM/M, necrotic muscle/muscle.

Scheme 1: Synthesis of ^{127}I-skyrin and ^{131}I-skyrin [a]

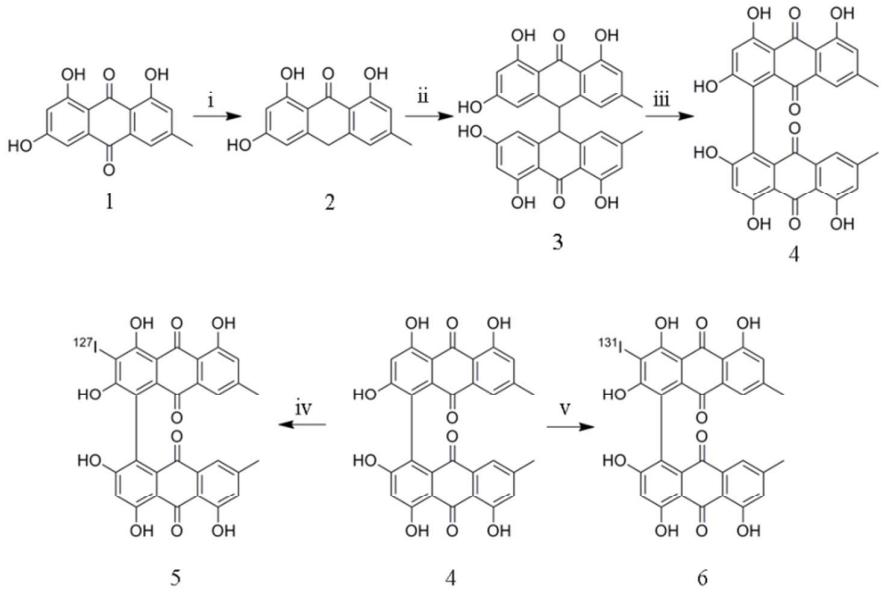

[a]Reagents and conditions: (i) $SnCl_2 \cdot 2H_2O$, HCl, CH_3COOH, 120 °C, 24 h; (ii) $FeCl_3 \cdot 6H_2O$, ethanol, reflux, 4 h; (iii) KOH, O_2, 120 °C, 10 min; (iv) I_2, THF and H_2O (1:1), $NaHCO_3$, 30 min; (v) $Na^{131}I$, Iodogen, 30 °C, 20 min.

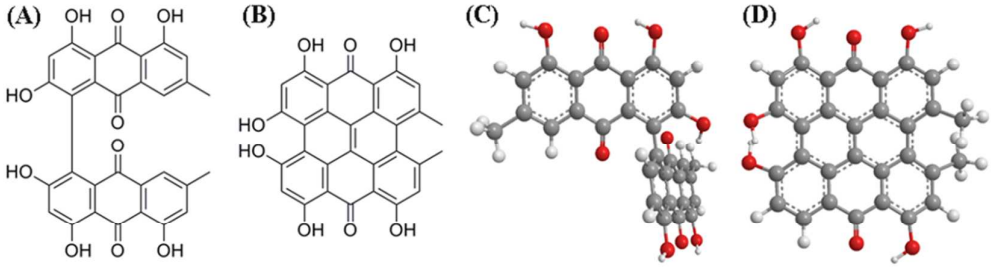

Figure 1: (A) Chemical structure of skyrin; (B) Chemical structure of Hyp; (C) three-dimensional space structure of skyrin; (D) three-dimensional space structure of Hyp.

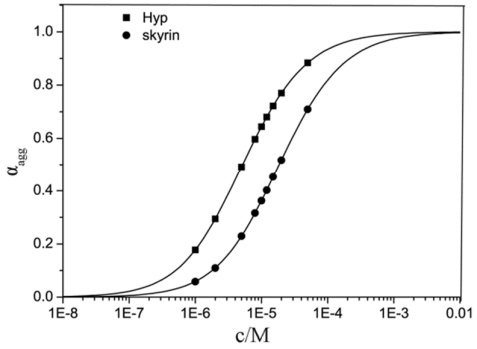

Figure 2: Fraction of aggregated molecules α_{agg} plotted as a function of concentration of skyrin or Hyp in 50% water-DMSO mixture (v/v). The lines were obtained by fitting the concentration-dependent UV/Vis data with the isodesmic model.

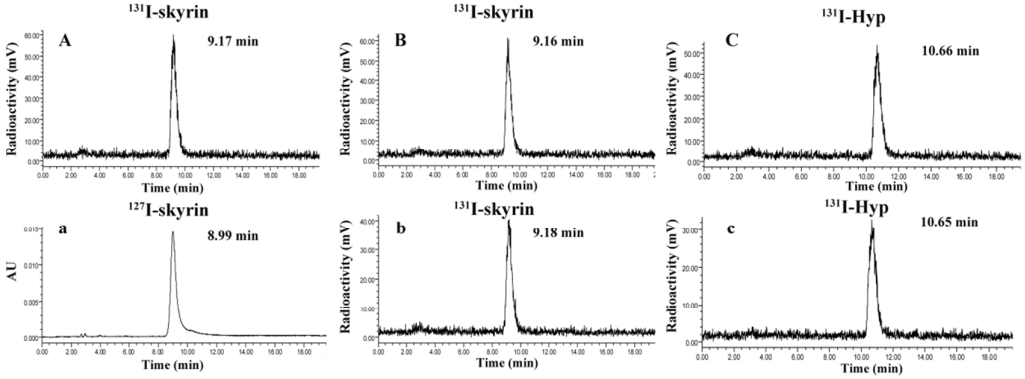

Figure 3: HPLC chromatograms of compounds of ^{127}I-skyrin (a), ^{131}I-skyrin (A) and the profiles of stability study of after incubation in rat plasma at 37 °C for 72 h (B and b, C and c) respectively. All the radiotracers were analyzed by using the isocratic HPLC method.

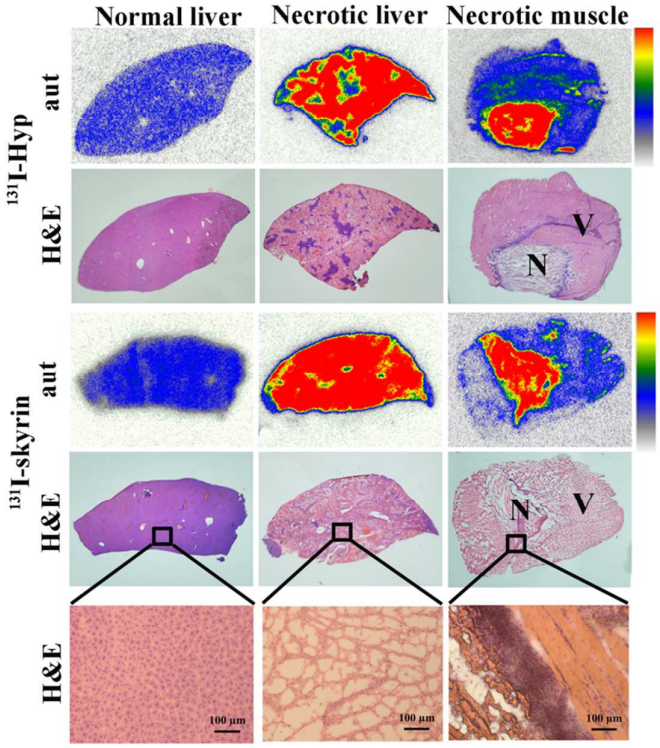

Figure 4: Representative autoradiograph (aut) and corresponding contrast-enhanced H&E images of 30 μm slices at 24 h after intravenous injection of ^{131}I-skyrin or ^{131}I-Hyp (14.8 MBq/kg). The high radioactivity regions seen on the autoradiogram match with the necrotic areas as verified by H&E stained slices. N = necrotic area, V = viable area. Scale bar = 100 μm.

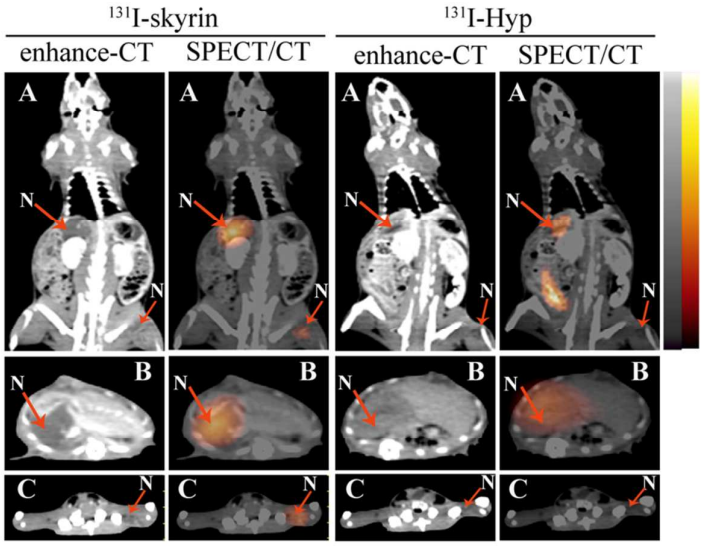

Figure 5: Representative enhanced CT and corresponding SPECT-CT images of rats with liver necrosis (large arrow) and muscle necrosis (small arrow) at 72 h after administration of 3.7 MBq of ^{131}I-skyrin or ^{131}I-Hyp. (A) Coronal section images. (B) Transverse section images of rat liver. (C) Transverse section images of rat hind limb. Red solid arrow pointed to the necrotic region of liver/muscle. N = necrotic area.

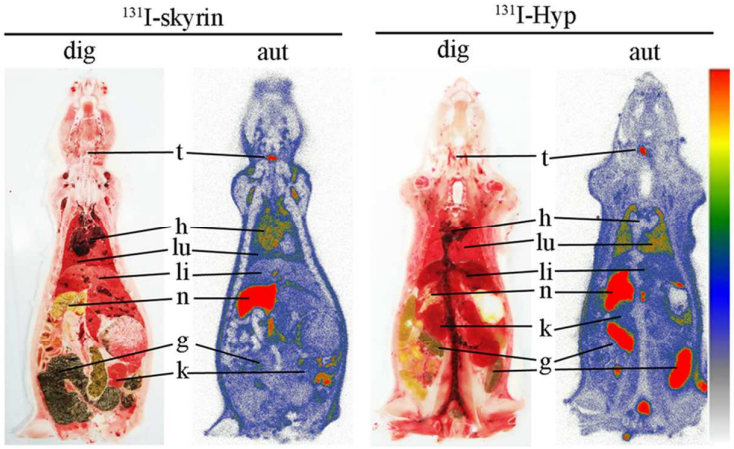

Figure 6: Representative whole body autoradiographic imaging of rats with liver necrosis and muscle necrosis at 72 h after administration of ^{131}I-skyrin or ^{131}I-Hyp to illustrate the biodistribution of the tracers. Both a digital photograph (dig) and a corresponding pseudocolored autoradiograph (aut) image are included for each tracer.

The following tissues are labeled in the image: thyroid (t), heart (h), lungs (lu), liver (li), necrotic liver (n), kidneys (k), and gut (g).

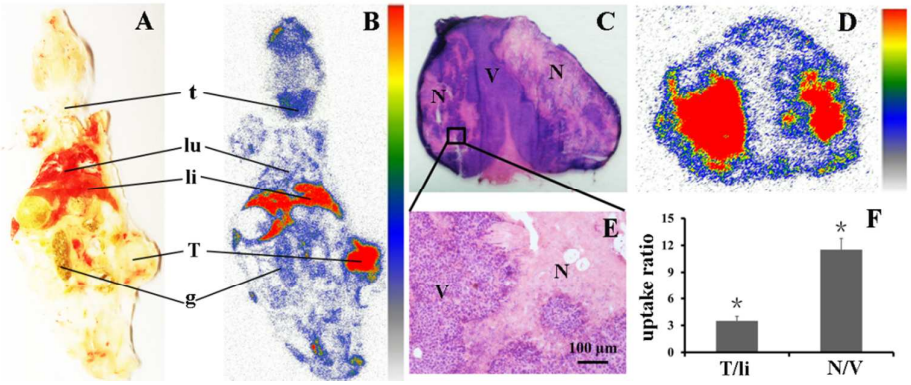

Figure 7: Mice were injected intravenously with ^{131}I-skyrin, (A) Representative whole body digital photograph. (B) Corresponding autoradiographic image. (C and E) Histopathological staining with H&E of excised tumors. (D) Representative autoradiographs of the same slide used in histopathological studies. (F) Uptake ratios of ^{131}I-skyrin determined by autoradiography. All images were acquired 72h after injection of ^{131}I-skyrin. The following tissues are labeled in the image: thyroid (t), lungs (lu), liver (li), tumor (T). N = necrotic area, V = viable area. Scale bar = 100 µm. *P < 0.05.

Table of Contents graphic